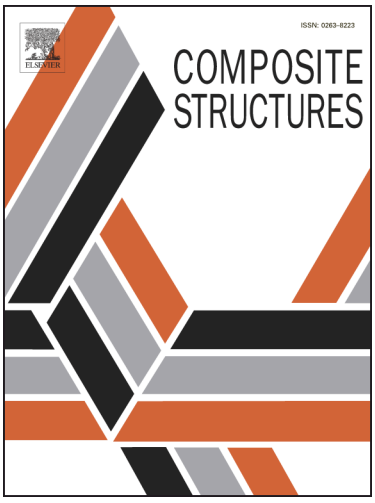

3D-printed Thermoplastic Composite Fasteners for Single Lap Joint Reinforcement

Wenhao Li, Shijun Guo, Ioannis K. Giannopoulos, Minxiao Lin, Yi Xiong, Yiding Liu, Zhengquan Shen

PII: S0263-8223(21)01505-1
DOI: https://doi.org/10.1016/j.compstruct.2021.115085
Reference: COST 115085

To appear in: *Composite Structures*

Received Date: 11 August 2021
Revised Date: 9 November 2021
Accepted Date: 4 December 2021

Please cite this article as: Li, W., Guo, S., Giannopoulos, I.K., Lin, M., Xiong, Y., Liu, Y., Shen, Z., 3D-printed Thermoplastic Composite Fasteners for Single Lap Joint Reinforcement, *Composite Structures* (2021), doi: https://doi.org/10.1016/j.compstruct.2021.115085

Composite Structures, Volume 282, February 2022, Article number 115085
DOI:10.1016/j.compstruct.2021.115085

3D-printed Thermoplastic Composite Fasteners for Single Lap Joint Reinforcement

Wenhao Li [a], Shijun Guo [a,*], Ioannis K. Giannopoulos [a], Minxiao Lin [a], Yi Xiong [b], Yiding Liu [c], Zhengquan Shen [a]

[a] Centre of Excellence for Aeronautics, School of Aerospace, Transport and Manufacturing, Cranfield University, Cranfield, MK43 0AL, UK.

[b] School of System Design and Intelligent Manufacturing, Southern University of Science and Technology, Shenzhen, 518055, China

[c] WMG, University of Warwick, Coventry, CV4 7AL, UK.

Abstract

This study presents findings for the strength and failure mechanism of a 3D-printed Continuous Carbon Fibre reinforced Onyx (CCF/Onyx) Thermo-Plastic Composite Fastener (TPCF) and a single lap-joint (SLJ) made of fibre/polymer composite reinforced by the TPCF. The study was carried out by numerical analysis and experiment methods including test sample design, manufacturing process and mechanical test. The 3D-printed fasteners were manufactured and tested in shear mode for two types of joining arrangement: fastened and hybrid bonded/fastened joints. Firstly, experiment was carried out for the TPCF fastened SLJ and the results show that addition of CCF in the Onyx matrix and post heat-treatment process could significant enhance the TPCF strength. The results was then benchmarked against a SLJ with steel fastening. The shear failure load of the SLJ reinforced by heat-treated CCF/Onyx TPCF of 8mm diameter was 36% lower than a SLJ reinforced by a steel bolt of the same size. Numerical model for progressive damage simulation was also created based on the failure theory from Puck and Schürmann achieving good correlation with the experimental data. Secondly, the TPCF fasteners were manufactured with two types of heat-treated countersunk head and pan head forming and used to reinforce bonded SLJ. The test results show that the bonded SLJ reinforced by the TPCF fastener of countersunk head is of 11.7% higher strength and an increase in ultimate deformation by 9.1% compared to a bonded SLJ reinforced by steel fastener of 5mm diameter. From the numerical and experimental study, it was noted that this was attributed to countersunk configuration to reduce out-out-plane bending and provide better crack arresting for the joint bonding.

Keywords: Thermoplastic Composite Fastener, 3D Printing, Single-lap Joint, Progressive Failure Model

*Corresponding author. E-mail address: s.guo@cranfield.ac.uk (S. Guo).

1. Introduction

Carbon Fibre Reinforced Polymer (CFRP) composites have been extensively used in the automotive, civil and aerospace industry due to the favourable high specific strength and stiffness material properties. Metallic fastening elements are still widely used either as the means to assemble composite material subcomponents or to complement the assembly of bonded structural assemblies. Fasteners offer a secondary load path in the failure case of the adhesive bond as well as providing increased structural strength and reliability to the assembled undamaged structure [1], [2]. The use of metallic fasteners undermine the potential of such assemblies to take advantage of the beneficial specific weight of composite materials. CFRP fasteners have shown great potential for replacing the conventional metallic fasteners in the hybrid bonded/fastened joints configurations [3]–[7]. They can provide with a weight benefit against using metallic fasteners, they are not susceptible to galvanic corrosion and, depending on the fastener design, they can exhibit higher specific strength compared to their metallic counterparts. Li et al. [3], investigated the feasibility of using CFRP pins as an alternative additional reinforcement to bonded/fastened single-lap joints. The work concluded that bonded single-lap joints, when reinforced by 8mm diameter composite pins, were able to reach a similar failure load to a bonded/fastened joint arrangement reinforced by a 5mm diameter steel fastener while achieving a 46% reduction in fastener weight. Guo and Li [4], investigated the failure mechanism and strength improvement of a sandwich composite T-joint reinforced by thermoplastic material fasteners subjected to pulling load. Based on the experimental results, the reinforced T-joint achieved nearly 19% improvement in the bonding strength compared to a purely bonded T-joint assembly. Ueda et al., manufactured and tested composite fasteners made from pultruded carbon fibre/PA66 commingled yarns, wrapped by glass fibre/PA6 [5]. Similarly, Fortier et al. manufactured and reshaped thermoplastic composite rivets from pultruded rods [6]. Yao et al. [7] extend the research to study the effect of matrix crystallinity and fibre content on fastener strength. The thermoplastic composite fasteners in the studies above have demonstrated their potential for applications in the aerospace industry, with the drawback of requiring complicated moulds and a time-consuming process for their application, which raises the production costs. Therefore, a more efficient fabrication and installation

process is necessary for further product industrialisation and the cost effective application of CFRP fasteners.

Additive Manufacturing (AM) process technique has attracted huge attention for structural applications in aerospace engineering and automotive industry [5, 6]. Fused deposition modelling (FDM) is a technique that allows a layer-by-layer built-up of components. Thermoplastic filaments feedstock is commonly used in FDM processes [10], such as Poly-Carbonate (PC), PolyLActide (PLA), PolyAmide (PA) and Acrylonitrile Butadiene Styrene (ABS) [8, 9]. However, the relatively poor part quality of FDM-based thermoplastic components, limits their application [13]. To improve the mechanical performance of FDM-fabricated pure thermoplastic parts [14], the filament feedstock is normally reinforced by various carbon fibres, such as nanofiber [11, 12], short fibre [13, 14, 15] and continuous fibre [20]–[28]. Among these, the 3D-printed continuous carbon Fibre Reinforced ThermoPlastic composites have reached, or even surpassed on occasions the properties of aerospace grade aluminium, which made them good candidates for primary structural load carrying component applications [20], [21]. Melenka et al [22], Tian et al [23], [24], Ning [25] and Van Der Klift et al. [26], investigated the influence of printing parameters such as layup sequence, filling density and fibre laydown pattern on the mechanical performance of 3D printed continuous carbon fibre reinforced composites. A comprehensive evaluation was conducted by Yang et al. [27] to explore the shear, flexural and tensile properties of 3D printed composites. The test results showed that by introducing a 10% by weight of continuous carbon fibre, the flexural strength and tensile strength increased significantly with respect to the pure thermoplastic material. For the state-of-the-art composite components manufactured by the AM technique, some factors have been identified as critical for the mechanical properties and performance of a finished part: the matrix and reinforcing fibre material; the bonding quality between fibres and matrix; the fibre alignment; the fibre homogeneity and porosity content.

The present study was focused on evaluating the strength of ThermoPlastic Composite Fasteners (TPCF) manufactured by 3D printing and Single Lap Joint (SLJ) reinforced by employing the TPCF. Experimental test was conducted to measure the shear strength of SLJs and the specimen out of plane displacement using digital image correlation. Subsequently, the failure mechanisms of the 3D printed fasteners were analysed through fracture surface inspection under Scanning Electron Microscope (SEM). In the same time, numerical model was created to simulate and provide further insight to the SLJ progressive failure behaviour by comparing the results with the test data.

2. Test sample preparation and experiment setup

2.1 TPCF manufactured by 3D printing

The TPCF test samples with full pan head at one end were fabricated using a desktop 3D printer (Mark Two, Mark Forged, Somerville, MA) as shown in figure 1. The 3D printer was equipped with dual extrusion head that allowed for separate printing as shown in figure 1(b) and (c), one to deposit the Onyx matrix (a Nylon filament strengthened with chopped carbon fibre, Mark Forged), and another for carbon fibre reinforced Nylon filament. The Onyx matrix was used in the outer fastener layer, at locations of high complexity and at thin regions where the carbon fibre filament could not be applied. The Onyx matrix was heated above its melting temperature and extruded from the nozzle onto the un-heated base panel, followed by continuous fibre deposition at a temperature higher than the melting temperature of the layer in process. Thus the matrix was melted interstitially between the continuous fibres. The fastener was made of 160 layers in total. Figure 2 shows the architecture of the 3D printed TPCF, where each layer was reinforced with concentric fibre rings/frames, limited by the part geometry and the matrix material was laid at a 45^{o} direction with respect to the fibres, alternating between plus and minus 45^{o} for each layer. The 3D printed fasteners were Onyx matrix based reinforced by carbon fibre filament having additional heat treatment. The heat treatment was a re-heating process to 200°C for 100 minutes and then cooling down in the oven to room temperature.

In the present study, the manufactured fastener was 20mm long with the body and the head 8mm and 16mm in diameter respectively. A blind hole of 10mm in depth and 1mm in diameter was fabricated in the centre of the other end of the fastener as shown in figure 1(d). This hole was prepared for the tail or head forming when applying the fastener to joint assembly. The heads were formed in cylindrical mould for pan head and conical mould for countersunk head.

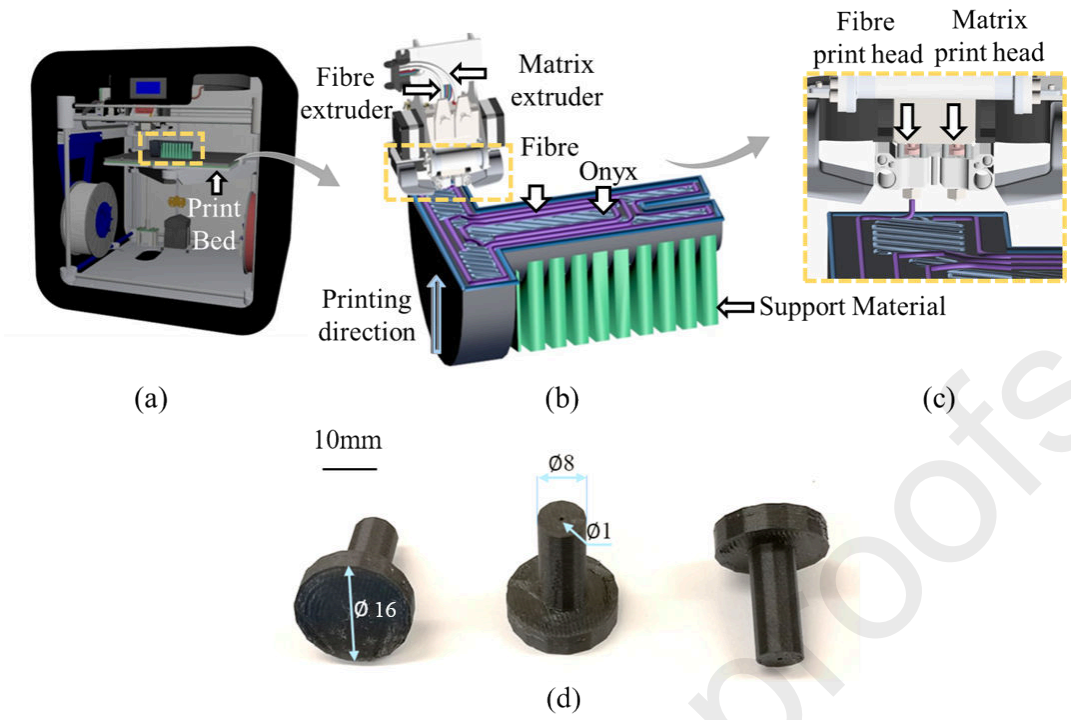

Figure 1. (a) The 3D printer, (b) the printed fastener, (c) the dual printer head, (d) Samples of 3D-printed TPCFs.

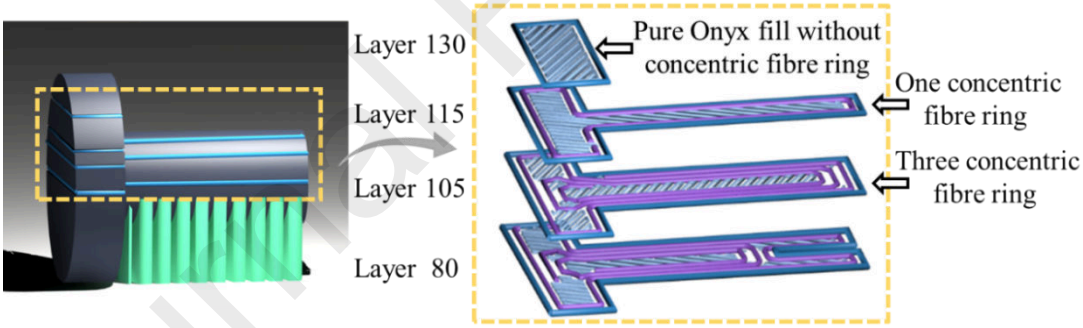

Figure 2. Architecture of the 3D printed TPCF and layer design schematics of the fibre/matrix reinforcement.

2.2 Single Lap Joint specimen design

Single lap joint test samples were manufactured from quasi-isotropic CFRP laminates made of 16 plies of carbon-epoxy prepreg (MTM46/HTS) in lay-up $[-45^o/0^o/45^o/90^o]_{2s}$ and total thickness 4.55mm as shown in figure 3(a). In the grip ends, doublers were made of the same material and layup and bonded to be in line with the end tabs of 0.8mm thickness made of aluminium alloy. Further details of the SLJ are listed in table 1, distinguished as purely fastened joint and bonded/fastened type. For the fastened only SLJs, a hole was drilled through the

centre of the joint overlap region and assembled by a fastener. These fasteners used in the test were of pan head type. For the bonded and bonded/fastened SLJs, the CFRP plates were initially bonded with Redux420® adhesive. The adhered region had an overlap splice length of 40mm and an average thickness of 0.2mm. Again, a hole was drilled in the centre of the overlap region and the fasteners were assembled to the bonded/fastened joint. Since the 3D printed fastener with heat treating exhibited better mechanical performance, the installed pan and countersunk fasteners were also heat-treated. A set of bonded/fastened samples using steel fasteners were also manufactured as baseline for comparison. Each of these bonded/bolted joint test samples are shown in figure 3(b).

Table 1. Types with some details of the SLJ test samples

SLJ type	Fastener types	Qty
Type-A. Fastened only	Type-1. 8mm Onyx fastener (Pan head)	3
	Type-2. 8mm CCF/Onyx fastener (Pan head)	3
	Type-3. 8mm CCF/Onyx with heat treatment (Pan head)	3
Type-B. Bonded/fastened	Type-3. 8mm CCF/Onyx with heat treatment (Pan head)	3
	Type-4. 8mm CCF/Onyx with heat treatment (countersunk head)	3
	Type-5. 5mm steel fastener	3

In the shear test of the SLJs, an INSTRON test machine equipped with a 100kN load cell as shown in figure 4 was employed at a loading rate of 1mm displacement/min until the SLJ failure. Three-dimensional Digital Image Correlation (3D-DIC) system was used to measure and correlate the out of plane displacement of the SLJ test sample with the simulation results.

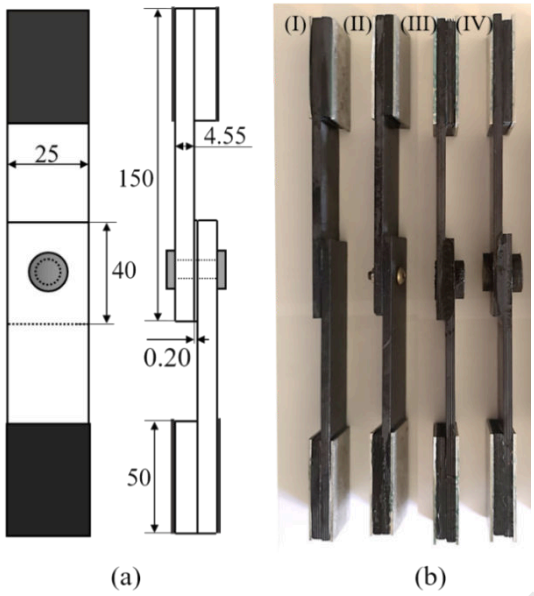

Figure 3. (a) SLJ dimensions, (b) (I) bonded joint, (II) bonded / 5mm steel fastener, (III) bonded / 8mm TPCF countersunk head, (IV) bonded / 8mm TPCF pan head

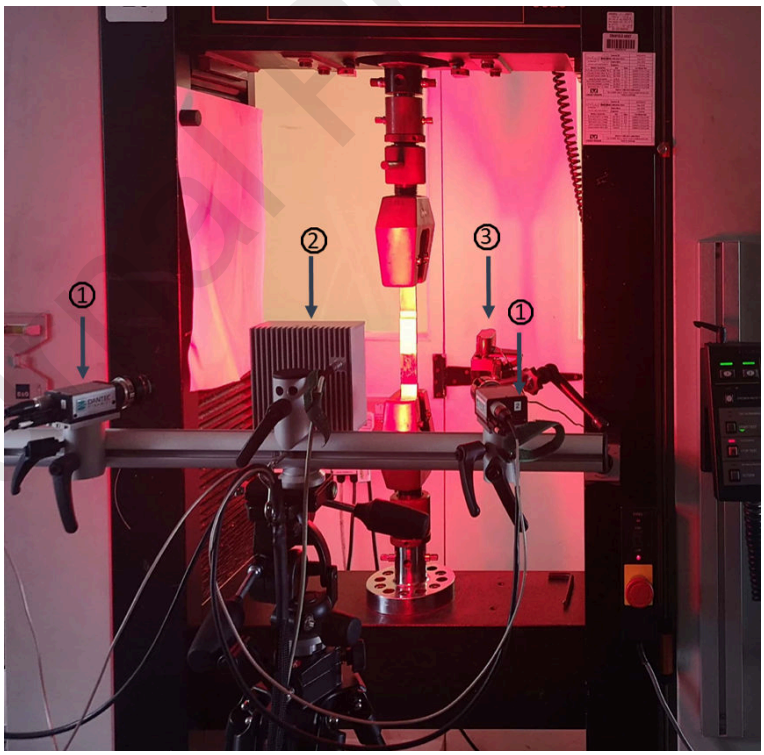

Figure 4. Experimental setup for the SLJ test with a digital correlation system, having two megapixel digital cameras (1), LED light (2) and one side camera (3).

2.3 Fastening process by thermal forming

To make the fastener's blank end forming to a required shape for joint assembly, the fastener shank was heated to the Onyx deflection temperature of 145°C and deformed by a forming tool according to the fastener head type, shown in figure 5(a) and (b). To form a pan head type, the blank end was heated and splayed by a tapered forming tool first, and then pressed into a hollow cylinder tool under constant pressure until cooling down. The countersunk head was formed by the tapered forming tool and the resulting head conical cavity was filled in by polymer. The head forming process lasted for 4 minutes, including half minute for material softening, half minute for part deformation and 3 minutes for cooling down. A pressure of 1.5 MPa was applied to form the composite fasteners' head until the heating reduced to room temperature. The head forming process for the two different types of composite fastener head is shown in Figure 5(c). The threaded M5 steel fastener was tightened by applying a torque of 3.4 Nm, which approximate equivalent to a 4.85 kN of preload.

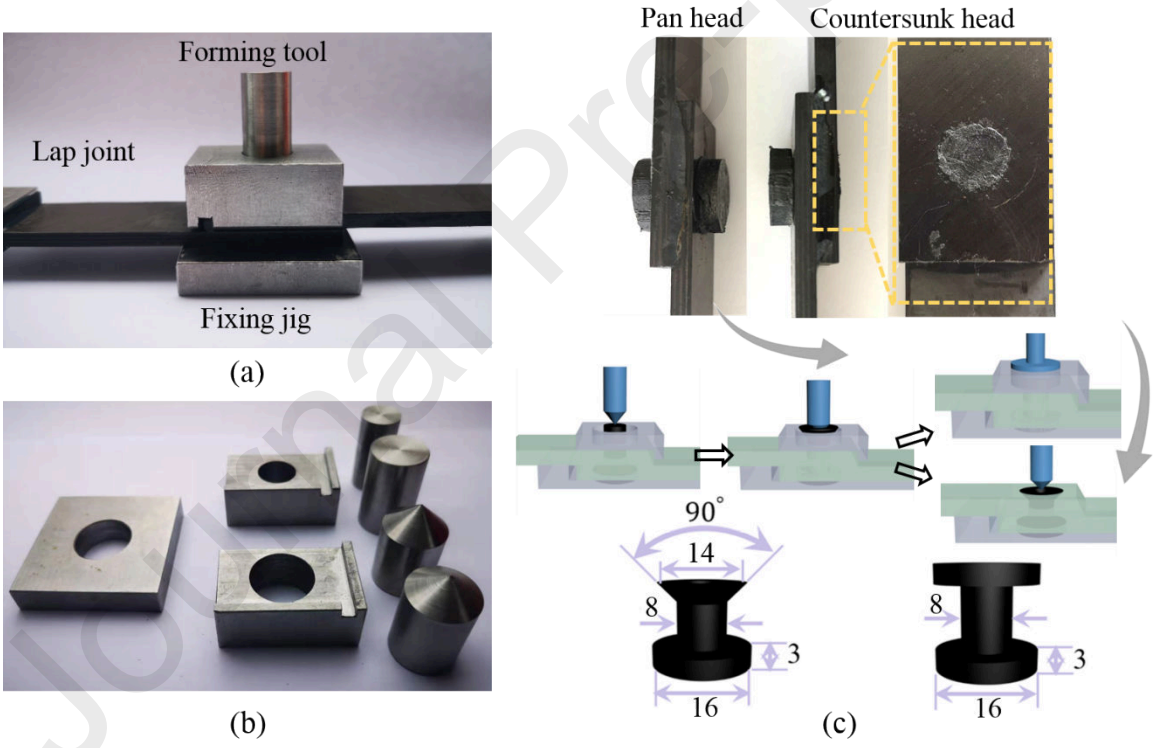

Figure 5. Fastening by thermal forming process including (a) forming tool set-up, (b) forming tools for different head type, (c) procedure and dimension of the formed TPCF.

3. Continuum Damage Model (CDM)

The 3D-pinted thermoplastic materials exhibit similar characteristic in terms of mechanical behaviour to the thermosetting composite materials with epoxy matrix that have been studied extensively. However, the failure mechanism and analysis have not yet been studied in the same level. For thermosetting composite materials, the World Wide Failure Exercise (WWFE) assessed 19 material failure theories for predicting the failure response [29]–[36]. The failure criterion from Hashin [28] has gained acceptance due to its relatively simple application, but it cannot accurately predict the failure modes governed by transverse compression, meaning compression perpendicular to the fibres direction. Puck and Schürmann failure criterion [35], developed based on a modified Mohr-Coulomb criterion, has shown promising failure predating performance in the failure under both transverse tension and compression by introducing the so called critical fracture plane. Proposed for orthotropic materials, the Puck and Schürmann failure criterion is suitable for 3D-printed composites, especially for continuous carbon fibre reinforced materials. However, originally developed for intrinsically brittle thermosetting materials, further modification and calibration on the failure model parameters is required for the more ductile thermoplastic composite materials. Gu and Chen [37] extended the Puck and Schürmann failure criterion to relate the crystallinity of thermoplastic materials with different transverse compression strength/transverse tensile strength ratio and inclination parameters. Based on this, Thiago Assis Dutra et al. [38] proposed a new fracture transition point based on original Puck and Schürmann failure criterion. The ratio between the transverse compressive strength and in-plane shear strength was investigated to take the effect of material crystallinity into consideration.

The failure analysis processes in the 3D-printed continuous carbon fibre reinforced materials are not that extensively researched as opposed to the unreinforced materials. In recent research works, a number of failure theories for the 3D-printed continuous carbon fibre reinforced material were carried out based on the Tsai-Hill anisotropic yield criterion [36], the Hashin damage criterion [37] and the Puck and Schürmann failure criterion [35]. In the current study, the Puck and Schürmann failure criterion is used for providing a benchmark study for the 3D-printed continuous carbon fibre reinforced composites failure assessment.

For the matrix and inter-fibre fracture, the Puck and Schürmann failure criterion was used to evaluate the fracture on the plane oriented at θ^o angle, as shown in Figure 6(a). A numerical

search was operated to determine the critical failure plane where the maximum stress exposure (f_E) occurs and calculate the stress σ_N, σ_T and σ_L on the plane as follows:

$$\sigma_n(\theta) = \sigma_{22}cos^2(\theta) + \sigma_{33}\, sin^2(\theta) + 2\,\tau_{23}sin(\theta)\, cos(\theta) \quad (1)$$

$$\tau_{nt}(\theta) = -\,\sigma_{22}\, sin(\theta)\, cos(\theta) \;+\; \sigma_{33}\, sin(\theta)\, cos(\theta) + \tau_{23}[cos^2(\theta) - sin^2(\theta)] \quad (2)$$

$$\tau_{n1}(\theta) = \tau_{13}sin(\theta) + \tau_{12}cos(\theta) \quad (3)$$

The stress exposure, f_E, indicates the risk of the material failure on a critical plane and $f_E \geq 1$ indicates a failure.

$$f_E = \begin{cases} \sqrt{(1-p_t)^2\left(\frac{\sigma_n}{Y_T}\right)^2 + \left(\frac{\tau_{n1}}{R_{n1}}\right)^2 + \left(\frac{\tau_{nt}}{R_{nt}}\right)^2} + p_t\frac{\sigma_n}{Y_T} \geq 1 \text{ for } \sigma_N \geq 0 \\ \sqrt{\left(p_c\frac{\sigma_n}{Y_c}\right)^2 + \left(\frac{\tau_{n1}}{R_{n1}}\right)^2 + \left(\frac{\tau_{nt}}{R_{nt}}\right)^2} + p_c\frac{\sigma_n}{Y_c} \geq 1 \text{ for } \sigma_N < 0 \end{cases} \quad (4)$$

Where p_t and p_c are inclination parameters, Y_t and Y_c are the tensile and compressive strength in the transverse direction, R_{n1} is the in-plane shear strength, R_{nt} is calculated as,

$$R_{nt} = Y_c cos^2(\theta_0) \quad (5)$$

Where θ_0 is the fracture angle in pure transverse compression test ($\theta_0 \approx 53^o$) [36].

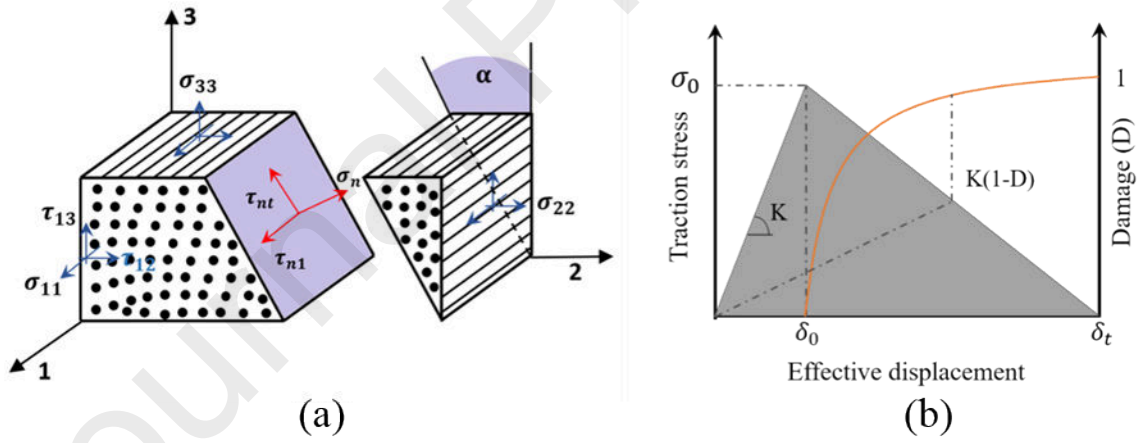

Figure 6. (a) Schematic of matrix compression failure where rotation performed to transfer the stress into the fracture plane. (b) Bi-linear softening damage law.

After damage initiation, a damage function can be established based on energy dissipation and bilinear softening law for post failure analysis, as shown in Figure 6(b). It assumed that the energy dissipation inside element under matrix failure equals to the mixed mode fracture toughness, G_T, which is the area under the bilinear damage evolution curve. A characteristic

element length is introduced into damage evolution expression. The damage function D can be expressed based on the linear softening law, from the point of initiation to final failure.

$$D = \frac{\delta_f(\delta - \delta_0)}{\delta(\delta_f - \delta_0)} - \tag{6}$$

Here, δ_0 represents the effective displacement at which the failure criterion is satisfied and δ_f is the effective displacement corresponding to the final failure. The effective displacement obtained from the effective strain and characteristic element length are defined as below,

$$\delta_{\text{eff}} = \begin{cases} \sqrt{\varepsilon_{\text{n}}^2 + \varepsilon_{\text{nt}}^2 + \varepsilon_{\text{nl}}^2} * l_c \text{ for } \sigma_N \geq 0 \\ \sqrt{\varepsilon_{\text{nt}}^2 + \varepsilon_{\text{nl}}^2} * l_c \text{ for } \sigma_N < 0 \end{cases} \tag{7}$$

Where ε_{n}, ε_t and ε_l are the material strain rotated to the fracture plane, l_c is the characteristic element length.

The δ_f is the final failure displacement defined by the mixed mode fracture toughness, G_T, the damage initiation effective stress (σ_{eff}^c).

$$\delta_f = \frac{2G_T}{\sigma_{\text{eff}}^c} \tag{8}$$

$$G_T = \frac{G_{IC}G_{IIC}(1 + \eta^2\lambda)}{G_{IIC} + G_{IC}\eta^2\lambda} \tag{9}$$

Where G_{IC} and G_{IIC} are the mode I and mode II delamination fracture toughness, λ is the equal to $\frac{G_{13}}{E_{22}}$,η is the relevant material coefficient defined as,

$$\eta = \frac{\sqrt{\varepsilon_{\text{nt}}^2 + \varepsilon_{\text{nl}}^2}}{\varepsilon_n} \tag{10}$$

For fibre fracture in tension or compression, Hashin damage criterion and bilinear softening law were used as described in [3], [4] and controlled in a similar way as shown in Figure 6 (b).

4. Numerical single-lap joint model

A numerical model was built to simulate the progressive failure of a single-lap joint (SLJ) reinforced by the 3D printed composite fastener using ABAQUS®/Explicit software. The FE mesh and boundary conditions set for the bonded SLJ reinforced by a fastener is shown in figure 7. Both adherents and fastener were modelled with three-dimensional solid elements C3D8R. The material failure subroutines were set based on the damage theory introduced in the above Section 3. Cohesive element COH3D8 was used in the adhesive bond layer with

element size set as one-fifth of the adjacent solid element [39], [40]. A summary of the material properties used in the FE model are listed on Table 2 and 3. The material data for MTM46/HTS and adhesive Redux420® were found in references [1, 2]. The elastic and damage properties of the 3D-printed composite materials used in this study were traced from [35, 36 and 37] where the same manufacturing process, filament material and fibre volume fraction were used. The printed TPCF model was assumed as having no voids and perfect fibre-matrix bonding with homogeneous transverse isotropic properties. The fracture toughness properties used for the printed TPCF were calibrated by using the test data [44]. Self-contact algorithm was employed between the fastener and hole to update contact pairs following the deletion of damaged elements.

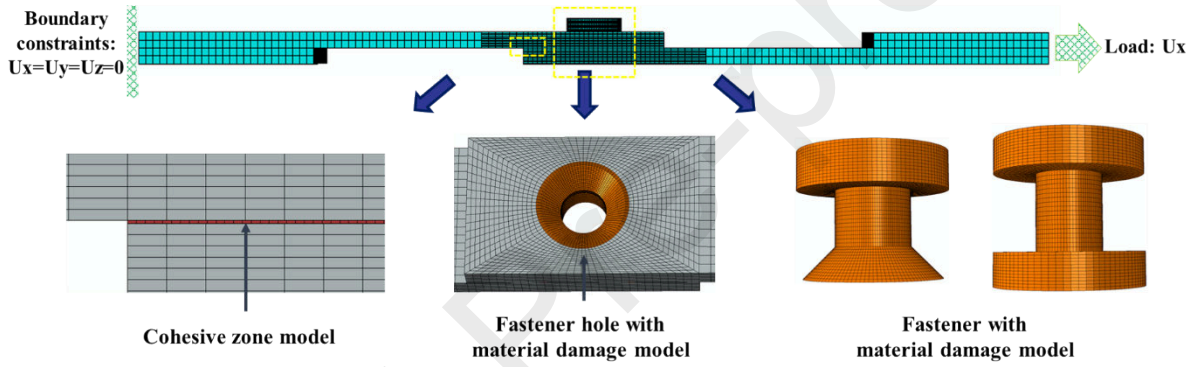

Figure 7. FE model and mesh of the bonded/fastened SLJ

Table 2 Material properties for 3D-printed TPCF and MTM46/HTS [35, 36 and 37]

Property	Units	Continuous fibre/onyx, 40% fibre volume fraction (fastener)	MTM46/HTS (joint laminates)
Axial Elastic Modulus, E11	[GPa]	68.08	128.30
Transverse Elastic Modulus, $E_{22}=E_{33}$	[GPa]	10.65	9
Axial Shear Modulus, $G_{12}=G_{13}$	[MPa]	2352	3950
Transverse Shear Modulus, G_{23}	[MPa]	2100	3500
Axial Poisson's Ratio, $\nu_{12}=\nu_{13}$	-	0.35	0.32

Axial Tension Strength, Xt	[MPa]	701.41	2278
Axial Compression Strength, Xc	[MPa]	223.06	1352
Transverse Tension Strength, Yt	[MPa]	33	33.90
Transverse Compression Strength, Yc	[MPa]	41.83	210
Shear Strength, S_{12}	[MPa]	44	98.10
Mode I delamination fracture toughness, G_{IC}	[N/mm]	3	0.22
Mode II delamination fracture toughness, G_{IIC}	[N/mm]	6	0.66
Fracture toughness in fibre tension, G_{FT}	[N/mm]	91.60	91.60
Fracture toughness in fibre tension, G_{FC}	[N/mm]	79.90	79.90

Table 3: Material properties for Adhesive Redux420®

Property	**Units**	**Adhesive Redux420® [1]**
Penalty Stiffness / normal direction	[N/mm^3]	2.40×10^5
Penalty Stiffness / shear direction	[N/mm^3]	9.20×10^4
Traction Strength / normal direction	[MPa]	10
Traction Strength / shear direction	[MPa]	15
SERR* / normal direction	[N/mm]	0.25
SERR* / shear direction	[N/mm]	0.67

*SERR: Strain Energy Release Rate or Fracture Toughness

5. Single Lap Joint Reinforced by the TPCF

5.1 Experimental results

The type-A single lap joint (SLJ) samples assembled by three types of 3D-printed TPCF were tested to evaluate the mechanical performance of the fastener against shear failure as shown in figure 8(a). The first set of type-A SLJ test samples were assembled by the type-1 fastener as classified in Table 1; the second set assembled by the type-2 fastener containing 40% volume of continuous carbon fibers; the third set was assembled by the type-3 fastener made use of type-2 fastener with additional heat treatment. The heat treatment was a post-process of re-heating the 3D printed TPCFs to 200°C for 100 minutes and then cooling down with oven to room temperature. The re-heating process was to enhance the chemical bonding between the matrix polymer chains and reduce the internal pore structure as shown in figure 8(b). As shown in figure 8(c), all TPCFs were sheared into two pieces at the fastener shank as a result of shear failure, while pull-through of the fastener heads was not observed. The results were compared with a SLJ reinforced by a pultruded carbon/epoxy thermosetting composite fastener of the same size (8mm diameter) as shown in figure 8(d). In addition, the test results were also compared with a similar SLJ connected by a steel fastener in previous study [3, 41]. A comparison of the above test results is shown in figure 9 where the average ultimate failure load with standard deviation of composite fastener are presented along with the specific strength of each type of joint.

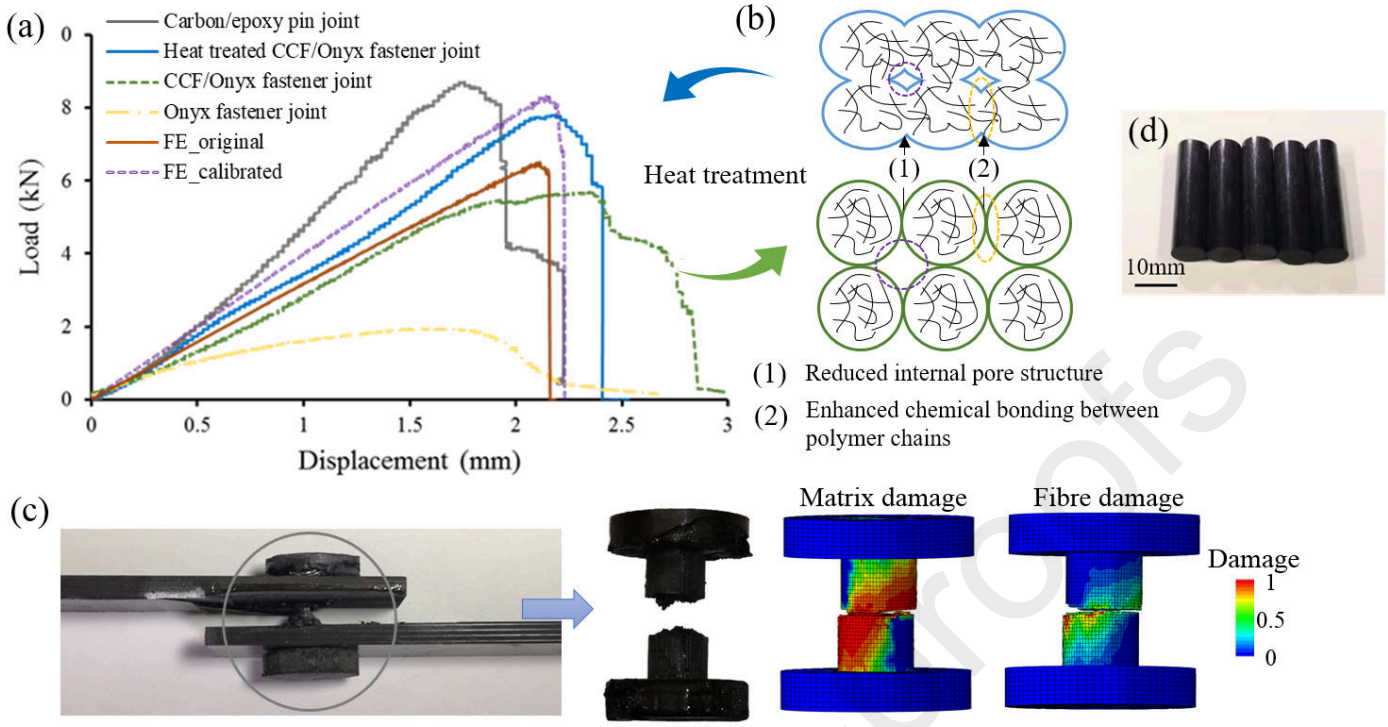

Figure 8: (a) Load-displacement test results of purely fastened SLJs, (b) schematic overview of the heat treatment effect on micro-structure, (c) the type-3 fastener failure (d) test samples of the carbon/epoxy fastener.

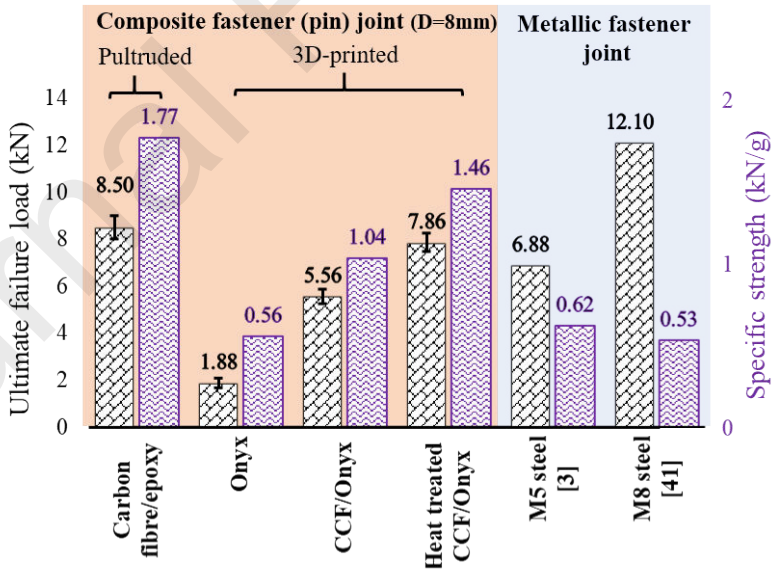

Figure 9: Ultimate failure load and specific strength of the Type-A joint reinforced by different types of fasteners.

5.2 Effect of fibre reinforcement and heat treatment on fastener mechanical properties

The type-2 fastener with added continuous carbon fibres (CCF) in the 3D printed type-1 fastener provided remarkable performance improvement. The test results of the SLJ using the type-1 TPCF show an average elastic stiffness of 1.74±0.04kN/mm and ultimate failure load of 1.88 kN±0.13kN. Compared with the type-1 fastener, the SLJ reinforced by the type-2 fastener without heat treatment resulted in a stiffness of 3.00±0.17kN/mm and ultimate failure load of 5.56 ± 0.35kN, which were increased by 73% and 196% respectively. The SLJ displacement under the ultimate failure load also reduced, which was attributed to the CCF added in the fastener. A similar trend of load-displacement relationship was reported in previous study by Masahito et al. [5] on SLJ reinforced by carbon/PA6 fastener with different fibre volume fraction.

The test results also demonstrated that the heat treatment post-process made further enhancement for the mechanical performance of the 3D printed TPCF. The measured stiffness of the SLJ reinforced by the type-3 TPCF was 3.62±1.78kN/mm and the ultimate failure load was 7.86± 0.39kN, which was increased by 20.35% and 41.37% respectively comparing with the SLJ reinforced by type-2 fastener without heat treatment. With regard to the elongation to failure, the type-2 fastener behaved more ductile with greater break elongation, while the type-3 fastener after post heat treatment fractured rapidly when reaching the maximum stress. This was closely related to the increased crystallinity of polymer induced by the heat treatment as reported in previous study [46], [47].

Moreover, the interface of polymer chains inside adjacent beads and interbead pore structure is one of the key properties to consider for a 3D-printed TPCF as shown in figure 8(b). Heat treatment not only increases the contact area between the printed beads and promoted the linking of polymer chains but also minimize the overall pore structure content. The fracture surface of a heat-treated CCF/Onyx fastener was dissected and exposed under a scanning electron microscope (SEM) for further investigation, shown in figure 10. Figure 10(a) is a representation close to the visual inspection level. It was noted that, the fracture pattern was very jagged with considerable matrix splitting, fibre pull-out and delamination. The delamination between deposited layers was enlarged and shown on figure 10(b) location (1). Some fibres were observed with a much cleaner break, figure10(c) location (2), while some were observed with fibre pull out, figure 10(d) location (3). After the heat treatment, the inter pore structural was nearly invisible, figure10(a) enlargement (4), which proved that the heat treatment effect on eliminating the porosity content.

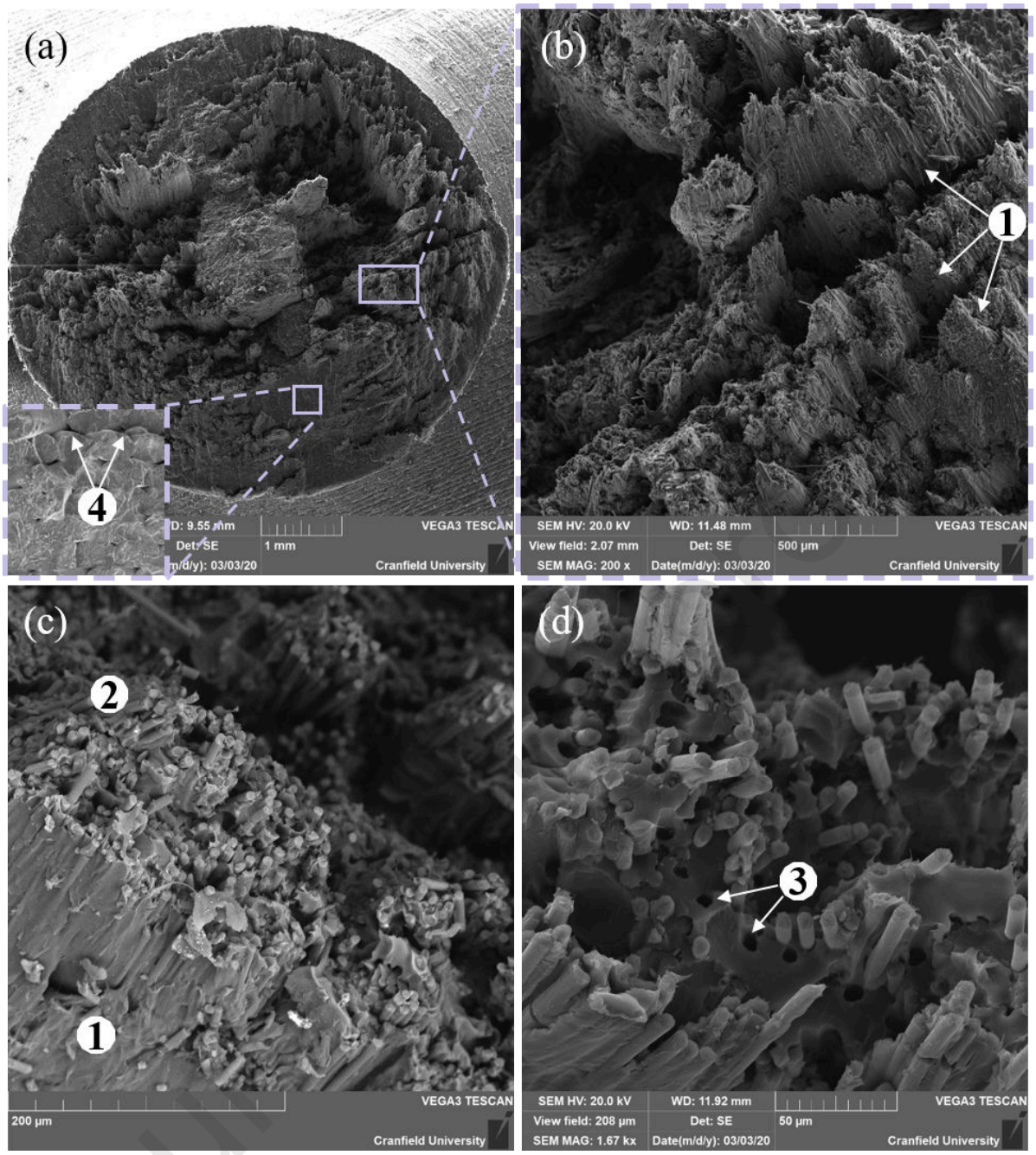

Figure 10. Fracture surface observed under SEM, (a) visual inspection level with (b), (c) and (d) successive image enlargement

5.3 Comparison between 3D-printed and pultruded composite fastener

The experimental results showed that the stiffness and ultimate strength of the SLJ reinforced by the 3D-printed type-3 fastener (CCF/Onyx with post heat treatment) was comparable but slightly lower than the baseline pultruded carbon/epoxy composite fastener [1]. The average ultimate failure load 7.86kN of type-3 fastener was 7.5% lower than the baseline fastener as shown in figure 9. The average joint stiffness of the type-3 fastener was 20% lower than the

baseline (4.87kN/mm). It was noted that the carbon fibre volume fraction of the baseline fastener was Vf≈50% according to measurement using optical microscopy.

The strength and stiffness of a 3D-printed composite reinforced by short carbon fibres can be increased up to 65% depending on short fibre length compared with the Nylon matrix [48]. Also, as reported by Easir and Anwarul [44] for example, by adding 5 wt% short fibre content in PLA matrix, the fracture toughness of the material was increased by 42% for [0/90] and 38% for [45/-45] bead orientation respectively. The 3D-printed composite reinforced by CCF is of lower mechanical properties even in the same fibre volume as the carbon/epoxy composite [42, 43]. An important reason was the lack of compaction stage in the manufacturing process that led to higher porosity in the printed part and reduced mechanical properties. Moreover, the CCF density in the state-of-the-art 3D printing technique is limited. For a printing path through area <2.5x1 mm^2, the gap was filled by Nylon matrix and made the property weak.

5.4 Comparison between composite and steel fasteners

Regarding the comparison with the SLJ assembled using a steel bolt, the ultimate failure load of the SLJ reinforced by the type-3 fastener (8mm diameter) was 36% lower than a steel opponent of the same size, but 14% higher than a steel opponent of 5mm diameter. While the ultimate failure load of the SLJ reinforced by pultruded carbon/epoxy composite fastener of 8mm diameter was 29.75% lower than a steel bolt of the same size, but 23.6% higher than that of a 5mm steel opponent. As shown in figure 9, the composite fastener has significantly higher specific strength than Grade 5 steel bolts. It is worth noting that composite joints reinforced by metallic fastener usually undergo bearing failure in gradual and progressive manner [3,4], whereas composite fasteners undergo shear mode dominated failure with fastener separation abruptly. Similar result was reported in [5], where the SLJs reinforced by steel fasteners exhibited severe bearing failure around the composite laminate bores. In contrast, the composite fastener fractured into two pieces without severe damage in the laminate hole.

5.5 Comparison between test data and simulation results

In order to evaluate the reliability and accuracy of the Puck and Schürmann failure criterion for the 3D-printed TPCF, the numerical simulation results were compared with the experiment results in figure 8(a). The results show that the stiffness and ultimate load were 3.05kN/mm and 6.33kN respectively with the mechanical properties in the FE model based on the type-2 fastener without post-heat-treated. The numerical results underestimated the joint stiffness and

strength of the type-3 fastener with heat-treatment. It was also noted that the Puck and Schürmann failure criterion was developed based on intrinsically brittle thermoset based composite materials rather than TPCF. The inclination parameters (p_t and p_c) in Equation (4) were obtained for the intrinsically brittle materials, as recommended by Puck et al. [50]. Therefore, an update of the inclination parameters is necessary for the TPCF especially with heat treatment that results in ductile-brittle transition of the polymer. In the present study, the material properties including the shear modulus (G_{12},) transverse compression strength (Yc) and delamination fracture energy (G_{IC} and G_{IIC}) used in the FE model were adjusted by a factor of 1.3, which was determined by fitting to the experimental data. The numerical model with the updated properties provided a better correlation with the test data for the SLJ reinforced by the type-3 fastener. According to the failure index results in figure 8(c), the fastener fractured in matrix failure dominated mode followed by fibre failure that agreed with the experiment results.

6. Bonded/fastened hybrid single-lap-joint

Experiment results of load-displacement from the type-B bonded/fastened hybrid joint reinforced by the type-3, type-4 and type-5 fasteners (see Table 1) are shown in figure 11. The hybrid joint reinforced by the type-4 TPCF (countersunk head) achieved the highest strength and failure displacement. The load-displacement of the joint test exhibited a linear relationship until reaching the failure load at point B, followed by an abrupt load drop and a non-linear residual force variation until the final failure at point C as shown in figure 11. The abrupt load drop occurred as a result of the adhesive shear failure and joint debonding. The strength and ultimate displacement were 11.7% and 9.2% larger than the joint reinforced by the type-5 steel fastener of 5mm diameter. The final joint failure at point C as shown in figure 11(c) was caused by the shear failure of the fastener with local bearing damage of the material being observed around the hole. The failure modes were successfully captured by the FE model. For the hybrid joint reinforced by the type-3 fastener (pan head), the load-displacement at point C showed a sudden drop as a result of shear dominated failure of the fastener. While, the joint reinforced by the type-4 fastener (countersunk head) exhibited a gradual drop of load towards point C as a result of shear failure of fastener and, especially, bearing failure around the hole.

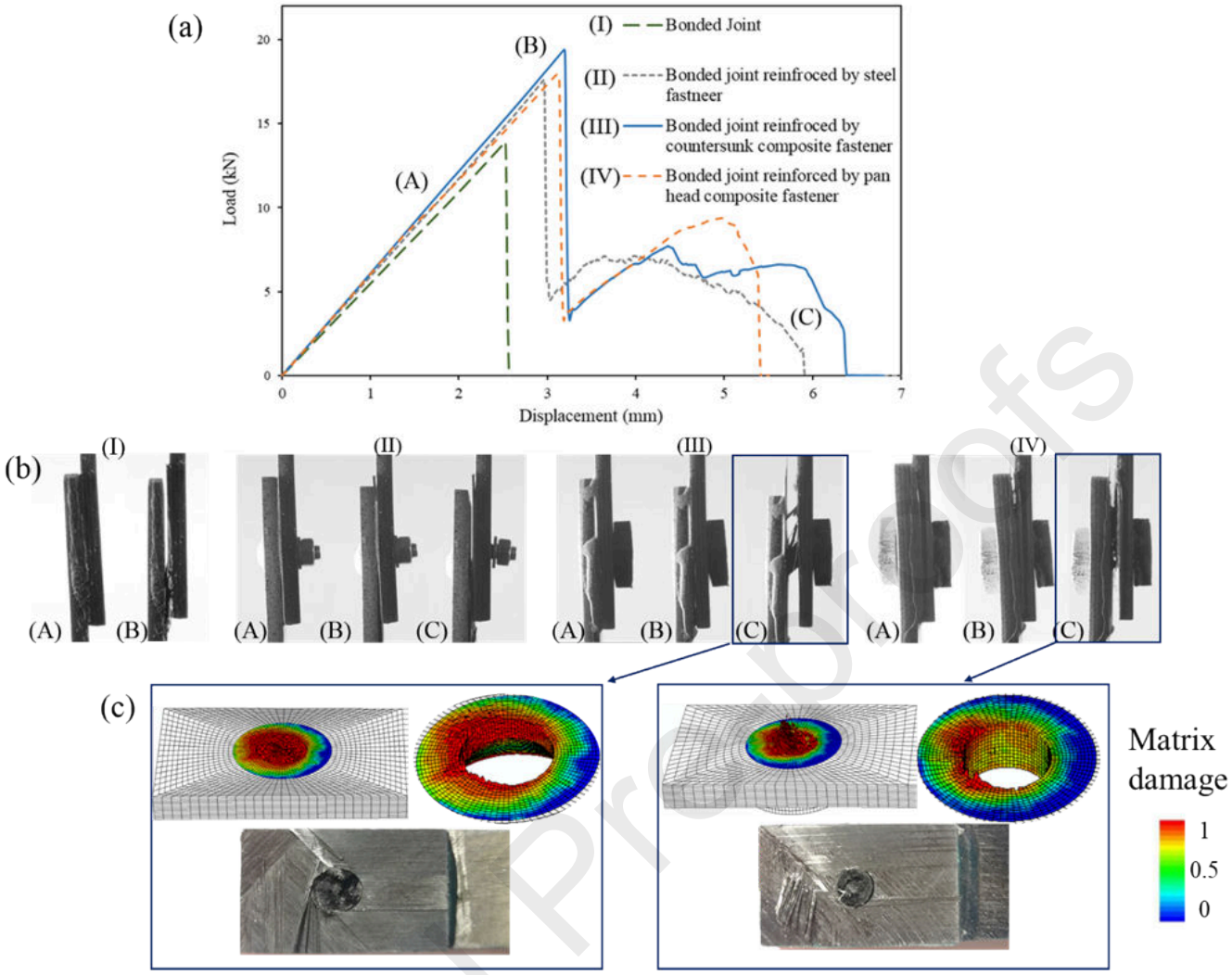

Figure 11. (a) Measured load-displacements of the type-B SLJ (b) failure of different SLJ samples (c) failure mode observed in the experiment and predicted by FE simulation

The average maximum load and failure displacement of each joint were measured as shown in figure 12. The results indicated that the fasteners provided additional load path for the joint after bonding interface failure. The strength of the joint was increased by 28.92%, 31.70% and 43.98%, and failure displacement was enhanced by 137.10%, 118.15% and 158.87% for the three types of fasteners respectively in comparison to a purely bonded baseline joint.

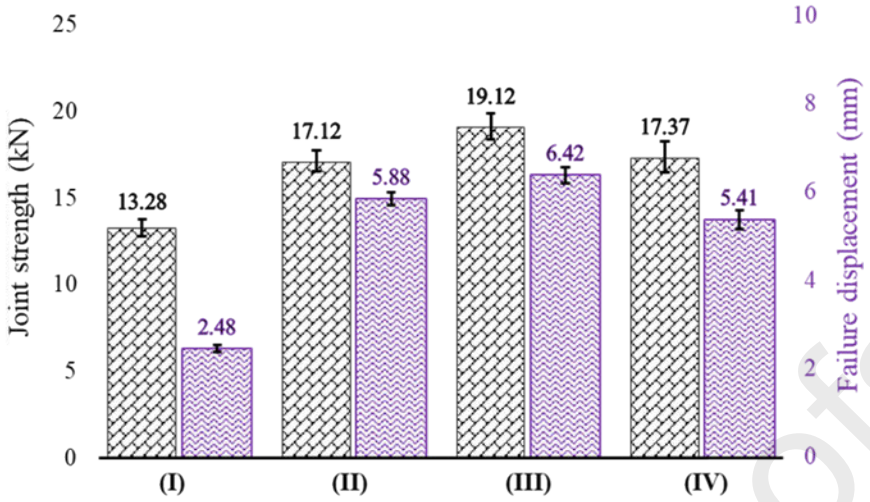

Figure 12. Strength and failure displacement of bonded/fastened joints.

The load-displacement results from the joint FE model are plotted to compare with the test data in figure 13, which shows the joint stiffness and ultimate load were predicted in acceptable accuracy. Meanwhile, the numerical model also successfully predicted the post-failure behaviour including the TPCF fracture and bearing failure following the joint debonding. The simulation of the joint reinforced by the type-5 steel fastener did not capture the full failure process because of excessive mesh distortion that terminated the simulation. The crack propagation in the joint bonding layer modelled by using the cohesive element with adhesive failure index counter map are plotted in figure 13, which were captured at 13 kN (see asterisk mark). Compared to the baseline purely bonded joint, the hybrid joints had less extent of adhesive damage. The fastener improved the joint damage tolerance and provided a crack arresting effect. In particular, the joint reinforced by the type-4 fastener exhibited better damage tolerance and the failure load was about 10% higher than the joint reinforced by the type-3 fastener and the steel bolt.

To evaluate the fastener type effect on the crack propagation and failure mode, the out-of-plane deformation field in the joint bonding region at load 13 kN was recorded by DIC as plotted in figure 13. The joint reinforced by the type-3 TPCF (pan head) and the type-5 fastener showed similar level of out-of-plane deformation, which was larger than the joint reinforced by the type-4 TPCF (countersunk head). The FE model-based simulation resulted in a similar trend. The results indicated that the type-4 TPCF (countersunk head) could reduce the joint secondary bending and lead to a stiffer joint due to smaller bolt-hole clearance and larger clamping force. The reduced secondary bending also mitigated the associated reaction between the fastener and the surrounding material of the hole, which could reduce the stress concentration.

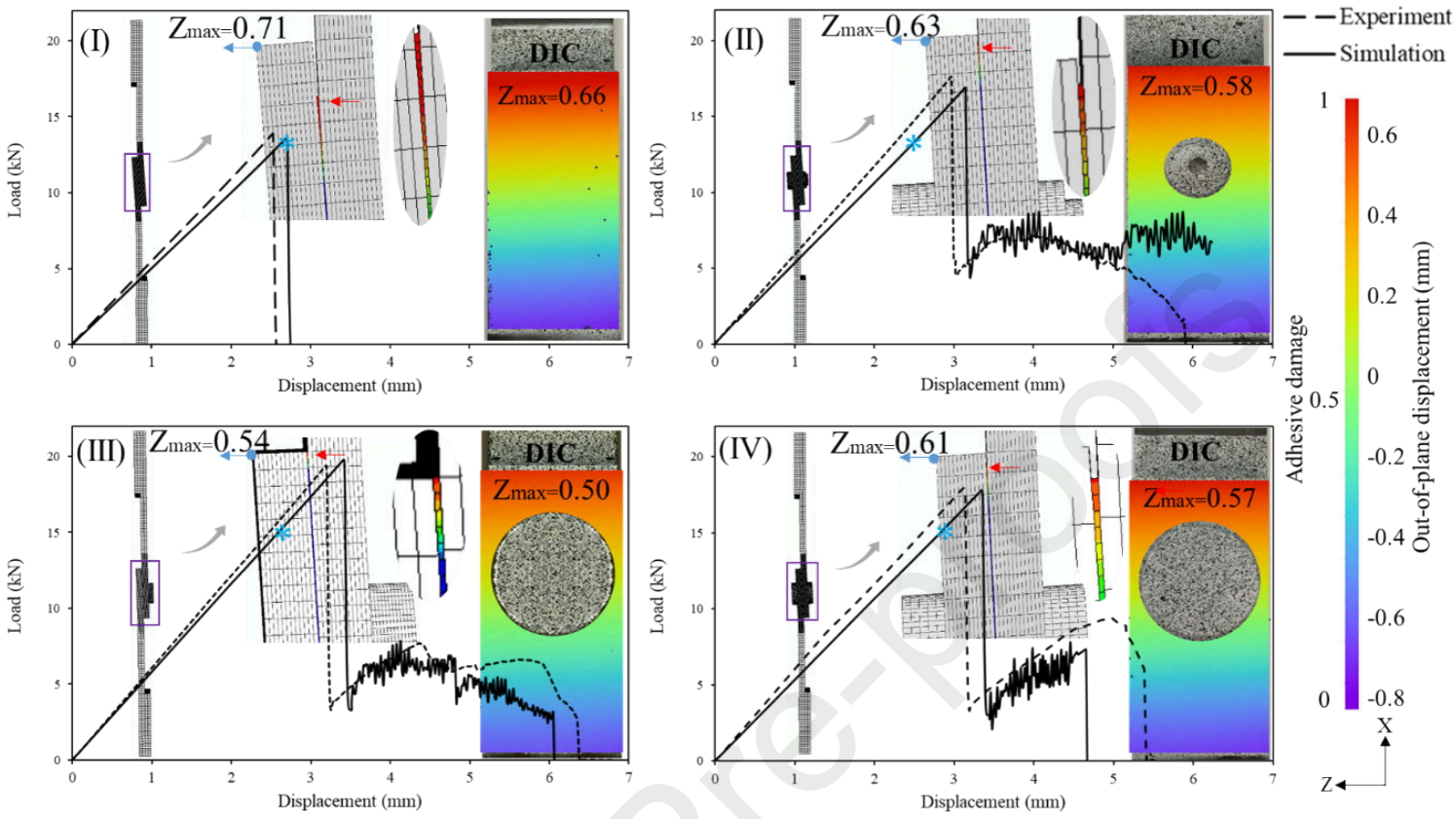

Figure 13. Load-displacement curve measured in experiment and predicted by FE model with out-of-plane displacement in the overlap region from DIC and simulation along with the crack propagation in adhesive under 13 kN loading.

Conclusions

This present research focused on the manufacturing of a proposed 3D printed TPCF including head forming and joint assembly process, and their mechanical properties and reinforcement for composite joints. Based on the experimental and numerical simulation results, the following conclusions are drawn.

- It was found that the stiffness and strength of a fastened only SLJ (type-A) assembled by using the 3D printed TPCF with 40% volume of CCF have significant increase (by 73% and 196% in the present example) comparing with the short-fibre reinforced TPCF.
- Further increase of stiffness and ultimate failure load (by 20.35% and 41.37% in presented example) can be achieved for the joint assembled by using the 3D printed CCF reinforced TPCF with post heat-treatment (type-3). The heat treatment led to increased crystallinity of polymer and enhanced interface properties between adjacent beads.

- The joint reinforced by 3D-printed TPCF with heat treatment demonstrated comparable mechanical performance to that by traditional carbon/epoxy thermosetting fastener, but under performed than a steel fastener of the same size.
- When employing the TPCF to reinforce a bonded SLJ (type-B), it was found that the joint reinforced by a TPCF of pan head (type-3) in 8 mm diameter achieved comparable mechanical performance to that of 5mm steel fastener.
- For the bonded SLJ, greater joint strength, stiffness and elongation to failure can be achieved by using the 3D-printed TPCF of countersunk head with heat-treatment (type-4) than its opponent of pan head (type-3). This was mainly attribute to minimized the contact clearance of the countersunk head with the hole and reduced out-of-plane bending.

Acknowledgement:

The authors acknowledge the financial support from China Scholarship Council (CSC NO. 201708140099). The authors also would like to extend the acknowledgements to Dr. Greg Gibbons for providing Mark two 3D printing machine to use.

Reference:

[1] G. Kelly, "Load transfer in hybrid (bonded/bolted) composite single-lap joints," *Compos. Struct.*, vol. 69, no. 1, pp. 35–43, 2005, doi: 10.1016/j.compstruct.2004.04.016.

[2] G. Kelly, "Quasi-static strength and fatigue life of hybrid (bonded/bolted) composite single-lap joints," *Compos. Struct.*, vol. 72, no. 1, pp. 119–129, 2006.

[3] W. Li, S. Guo, I. K. Giannopoulos, S. He, and Y. Liu, "Strength enhancement of bonded composite laminate joints reinforced by composite Pins," *Compos. Struct.*, vol. 236, p. 111916, Mar. 2020, doi: 10.1016/j.compstruct.2020.111916.

[4] S. Guo and W. Li, "Numerical analysis and experiment of sandwich T-joint structure reinforced by composite fasteners," *Compos. Part B Eng.*, vol. 199, p. 108288, Oct. 2020, doi: 10.1016/j.compositesb.2020.108288.

[5] M. Ueda, N. Ui, and A. Ohtani, "Lightweight and anti-corrosive fiber reinforced thermoplastic rivet," *Compos. Struct.*, vol. 188, pp. 356–362, 2018.

[6] V. Fortier, J.-E. Brunel, and L. L Lebel, "Fastening composite structures using braided thermoplastic composite rivets," *J. Compos. Mater.*, p. 0021998319867375, 2019.

[7] C. Yao, Z. Qi, W. Chen, C. Z.-C. P. B. Engineering, and undefined 2021, "Experimental study on CF/PEEK thermoplastic fastener: Effects of fastener matrix crystallinity and fibre content on the strength of single-lap joint," *Elsevier*,

Accessed: Mar. 29, 2021. [Online]. Available: https://www.sciencedirect.com/science/article/pii/S1359836821001293.

[8] F. Rengier *et al.*, "3D printing based on imaging data: review of medical applications," *Int. J. Comput. Assist. Radiol. Surg.*, vol. 5, no. 4, pp. 335–341, 2010.

[9] B. Berman, "3-D printing: The new industrial revolution," *Bus. Horiz.*, vol. 55, no. 2, pp. 155–162, 2012.

[10] H. L. Tekinalp *et al.*, "Highly oriented carbon fiber–polymer composites via additive manufacturing," *Compos. Sci. Technol.*, vol. 105, pp. 144–150, 2014.

[11] P. Dudek, "FDM 3D printing technology in manufacturing composite elements," *Arch. Metall. Mater.*, vol. 58, no. 4, pp. 1415–1418, 2013.

[12] L. Novakova-Marcincinova, J. Novak-Marcincin, J. Barna, and J. Torok, "Special materials used in FDM rapid prototyping technology application," in *2012 IEEE 16th International Conference on Intelligent Engineering Systems (INES)*, 2012, pp. 73–76.

[13] G. Liu, Y. Xiong, L. Z.-C. Communications, and undefined 2021, "Additive manufacturing of continuous fiber reinforced polymer composites: Design opportunities and novel applications," *Elsevier*, Accessed: Nov. 10, 2021. [Online].

[14] W. Zhong, F. Li, Z. Zhang, L. Song, and Z. Li, "Short fiber reinforced composites for fused deposition modeling," *Mater. Sci. Eng. A*, vol. 301, no. 2, pp. 125–130, 2001.

[15] M. Tarfaoui, A. El Moumen, and K. Lafdi, "Progressive damage modeling in carbon fibers/carbon nanotubes reinforced polymer composites," *Compos. Part B Eng.*, vol. 112, pp. 185–195, 2017.

[16] J. M. Gardner *et al.*, "Additive manufacturing of multifunctional components using high density carbon nanotube yarn filaments," 2016.

[17] B. Brenken, E. Barocio, A. Favaloro, V. Kunc, and R. B. Pipes, "Fused filament fabrication of fiber-reinforced polymers: A review," *Addit. Manuf.*, vol. 21, pp. 1–16, 2018.

[18] F. Ning, W. Cong, J. Qiu, J. Wei, and S. Wang, "Additive manufacturing of carbon fiber reinforced thermoplastic composites using fused deposition modeling," *Compos. Part B Eng.*, vol. 80, pp. 369–378, 2015.

[19] R. T. L. Ferreira, I. C. Amatte, T. A. Dutra, and D. Bürger, "Experimental characterization and micrography of 3D printed PLA and PLA reinforced with short carbon fibers," *Compos. Part B Eng.*, vol. 124, pp. 88–100, 2017.

[20] A. N. Dickson, J. N. Barry, K. A. McDonnell, and D. P. Dowling, "Fabrication of continuous carbon, glass and Kevlar fibre reinforced polymer composites using additive manufacturing," *Addit. Manuf.*, vol. 16, pp. 146–152, 2017.

[21] K. Mori, T. Maeno, and Y. Nakagawa, "Dieless forming of carbon fibre reinforced plastic parts using 3D printer," *Procedia Eng.*, vol. 81, pp. 1595–1600, 2014.

[22] G. W. Melenka, B. K. O. Cheung, J. S. Schofield, M. R. Dawson, and J. P. Carey, "Evaluation and prediction of the tensile properties of continuous fiber-reinforced 3D printed structures," *Compos. Struct.*, vol. 153, pp. 866–875, 2016.

[23] X. Tian, T. Liu, C. Yang, Q. Wang, and D. Li, "Interface and performance of 3D printed continuous carbon fiber reinforced PLA composites," *Compos. Part A Appl. Sci. Manuf.*, vol. 88, pp. 198–205, 2016.

[24] X. Tian, T. Liu, Q. Wang, A. Dilmurat, D. Li, and G. Ziegmann, "Recycling and remanufacturing of 3D printed continuous carbon fiber reinforced PLA composites," *J. Clean. Prod.*, vol. 142, pp. 1609–1618, Jan. 2017, doi: 10.1016/j.jclepro.2016.11.139.

[25] F. Ning, W. Cong, Y. Hu, and H. Wang, "Additive manufacturing of carbon fiber-reinforced plastic composites using fused deposition modeling: Effects of process parameters on tensile properties," *J. Compos. Mater.*, vol. 51, no. 4, pp. 451–462, 2017.

[26] F. Van Der Klift, Y. Koga, A. Todoroki, M. Ueda, Y. Hirano, and R. Matsuzaki, "3D printing of continuous carbon fibre reinforced thermo-plastic (CFRTP) tensile test specimens," *Open J. Compos. Mater*, vol. 6, no. 1, pp. 18–27, 2016.

[27] C. Yang, X. Tian, T. Liu, Y. Cao, and D. Li, "3D printing for continuous fiber reinforced thermoplastic composites: mechanism and performance," *Rapid Prototyp. J.*, vol. 23, no. 1, pp. 209–215, 2017.

[28] J. Naranjo-Lozada, H. Ahuett-Garza, P. Orta-Castañón, W. M. H. Verbeeten, and D. Sáiz-González, "Tensile properties and failure behavior of chopped and continuous carbon fiber composites produced by additive manufacturing," *Addit. Manuf.*, vol. 26, pp. 227–241, 2019.

[29] Y.-X. Zhou and Z.-M. Huang, "A bridging model prediction of the ultimate strength of composite laminates subjected to triaxial loads," *J. Compos. Mater.*, vol. 46, no. 19–20, pp. 2343–2378, 2012.

[30] N. Carrere, F. Laurin, and J. F. Maire, "Micromechanical-based hybrid mesoscopic 3D approach for non-linear progressive failure analysis of composite structures," *J. Compos. Mater.*, vol. 46, no. 19–20, pp. 2389–2415, 2012.

[31] E. E. Nelson, A. C. Hansen, and J. Steven Mayes, "Failure analysis of composite laminates subjected to hydrostatic stresses: A multicontinuum approach," *J. Compos. Mater.*, vol. 46, no. 19–20, pp. 2461–2483, 2012.

[32] Z. Hashin, "Failure criteria for unidirectional fiber composites," *J. Appl. Mech.*, vol. 47, no. 2, pp. 329–334, 1980.

[33] S. T. Pinho, R. Darvizeh, P. Robinson, C. Schuecker, and P. P. Camanho, "Material and structural response of polymer-matrix fibre-reinforced composites," *J. Compos. Mater.*, vol. 46, no. 19–20, pp. 2313–2341, 2012.

[34] H. M. Deuschle and A. Puck, "Application of the Puck failure theory for fibre-reinforced composites under three-dimensional stress: Comparison with experimental results," *J. Compos. Mater.*, vol. 47, no. 6–7, pp. 827–846, 2013.

[35] A. Puck and H. Schürmann, "Failure analysis of FRP laminates by means of physically based phenomenological models," in *Failure Criteria in Fibre-Reinforced-Polymer Composites*, Elsevier, 2004, pp. 832–876.

[36] C. G. Davila, P. P. Camanho, and C. A. Rose, "Failure criteria for FRP laminates," *J. Compos. Mater.*, vol. 39, no. 4, pp. 323–345, 2005.

[37] J. Gu and P. Chen, "Extension of Puck's inter fibre fracture (IFF) criteria for UD composites," *Compos. Sci. Technol.*, vol. 162, pp. 79–85, Jul. 2018, doi: 10.1016/j.compscitech.2018.04.019.

[38] T. A. Dutra, R. T. L. Ferreira, H. B. Resende, B. J. Blinzler, and R. Larsson, "Expanding Puck and Schürmann Inter Fiber Fracture Criterion for Fiber Reinforced Thermoplastic 3D-Printed Composite Materials," *Materials (Basel).*, vol. 13, no. 7, p. 1653, Apr. 2020, doi: 10.3390/ma13071653.

[39] Y. Liu, X. Zhang, S. Lemanski, H. Y. Nezhad, and D. Ayre, "Experimental and numerical study of process-induced defects and their effect on fatigue debonding in composite joints," *Int. J. Fatigue*, vol. 125, pp. 47–57, Aug. 2019, doi: 10.1016/j.ijfatigue.2019.03.033.

[40] Y. Liu, S. Lemanski, X. Zhang, D. Ayre, and H. Y. Nezhad, "A finite element study of fatigue crack propagation in single lap bonded joint with process-induced disbond," *Int. J. Adhes. Adhes.*, vol. 87, pp. 164–172, Dec. 2018, doi: 10.1016/j.ijadhadh.2018.10.005.

[41] J. Justo, L. Távara, L. García-Guzmán, and F. París, "Characterization of 3D printed long fibre reinforced composites," *Compos. Struct.*, vol. 185, pp. 537–548, Feb. 2018, doi: 10.1016/j.compstruct.2017.11.052.

[42] H. Al Abadi, H. T. Thai, V. Paton-Cole, and V. I. Patel, "Elastic properties of 3D printed fibre-reinforced structures," *Compos. Struct.*, vol. 193, pp. 8–18, Jun. 2018, doi: 10.1016/j.compstruct.2018.03.051.

[43] H. Zhang *et al.*, "Failure analysis of 3D printed woven composite plates with holes under tensile and shear loading," *Compos. Part B Eng.*, vol. 186, p. 107835, Apr. 2020, doi: 10.1016/j.compositesb.2020.107835.

[44] E. A. Papon and A. Haque, "Fracture toughness of additively manufactured carbon fiber reinforced composites," *Addit. Manuf.*, vol. 26, pp. 41–52, Mar. 2019, doi: 10.1016/j.addma.2018.12.010.

[45] H. Cui, Y. Li, Y. Liu, J. Guo, and Q. Xu, *Numerical simulation of composites joints failure based on cohesive zone model*, vol. 27. 2010.

[46] C. Yang, X. Tian, D. Li, Y. Cao, F. Zhao, and C. Shi, "Influence of thermal processing conditions in 3D printing on the crystallinity and mechanical properties of PEEK material," *J. Mater. Process. Technol.*, vol. 248, pp. 1–7, Oct. 2017, doi: 10.1016/j.jmatprotec.2017.04.027.

[47] P. Geng *et al.*, "Effect of Thermal Processing and Heat Treatment Condition on 3D Printing PPS Properties," *Polymers (Basel).*, vol. 10, no. 8, p. 875, Aug. 2018, doi: 10.3390/polym10080875.

[48] L. G. Blok, M. L. Longana, H. Yu, and B. K. S. Woods, "An investigation into 3D printing of fibre reinforced thermoplastic composites," *Addit. Manuf.*, vol. 22, pp. 176–186, Aug. 2018, doi: 10.1016/j.addma.2018.04.039.

[49] X. Wang, M. Jiang, Z. Zhou, J. Gou, and D. Hui, "3D printing of polymer matrix composites: A review and prospective," *Composites Part B: Engineering*, vol. 110. Elsevier Ltd, pp. 442–458, Feb. 01, 2017, doi: 10.1016/j.compositesb.2016.11.034.

[50] A. Puck, J. Kopp, and M. Knops, "Guidelines for the determination of the parameters in Puck's action plane strength criterion," *Compos. Sci. Technol.*, vol. 62, no. 3, pp. 371–378, Feb. 2002, doi: 10.1016/S0266-3538(01)00202-0.

Figure list:

CRediT authorship contribution statement

Wenhao. Li: Formal analysis, Data curation, Experiment, Validation, Software, Writing - original draft, Writing - review & editing. **Shijun. Guo:**

Conceptualization, Methodology, Validation, Funding acquisition, Resources, Writing - review & editing, Supervision.**Ioannis K. Giannopoulos:** Writing - review & editing. **Minxiao Lin:** Experiment.**Yi Xiong:** Experiment, Validation. **Yiding Liu:** Writing - review & editing. **Zhengquan Shen:** Writing - review & editing.

The authors declare that they have no known competing financial interests or personal relationships that could have appeared to influence the work reported in this paper.

3D-printed thermoplastic composite fasteners for single lap joint reinforcement

Li, Wenhao

2021-12-10

Li W, Guo S, Giannopoulos IK, et al., (2022) 3D-printed thermoplastic composite fasteners for single lap joint reinforcement. Composite Structures, Volume 282, February 2022, Article number 115085

https://doi.org/10.1016/j.compstruct.2021.115085